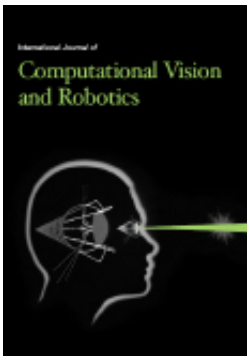


**International Journal of Computational Vision and Robotics**

ISSN online: 1752-914X - ISSN print: 1752-9131
https://www.inderscience.com/ijcvr

# High-speed optical 3D measurement device for quality control of aircraft rivet

Benjamin Bringier, Majdi Khoudeir

**DOI:** 10.1504/IJCVR.2022.10050711

**Article History:**

| | |
|---|---|
| Received: | 04 October 2021 |
| Accepted: | 20 April 2022 |
| Published online: | 01 December 2023 |

# High-speed optical 3D measurement device for quality control of aircraft rivet

Benjamin Bringier* and Majdi Khoudeir

University of Poitiers CNRS,
XLIM, UMR 7252, France
Email: benjamin.bringier@univ-poitiers.fr
Email: majdi.khoudeir@univ-poitiers.fr
*Corresponding author

**Abstract:** Optical three-dimensional devices are widely used for quality control in the industry and allow controlling various defects or properties. In the context of aeronautics, quality control of the parts' assembly is problematic due to the number of rivets to be checked and the necessary measurement accuracy. This paper presents a new device that makes it possible to measure the positioning of a rivet in less than two seconds with a measurement accuracy close to 10 $\mu$m. A standard colour camera and a projector are used to achieve a relatively low-cost device. This device is lightweight and compact enough to be mounted on a robotic arm. Few parameters must be calibrated, and the proposed methodology is accurate even if device positioning errors occur or the appearance of the surface is changed. From a single image acquisition, about 2,000 measuring points on the aircraft skin and up to 600 measuring points on a rivet head of 1 $cm^2$ are performed to evaluate its positioning. Our device is validated by a comparative approach and in real conditions of use.

**Keywords:** optical three-dimensional device; computer vision; image processing; quality control.

**Reference** to this paper should be made as follows: Bringier, B. and Khoudeir, M. (2024) 'High-speed optical 3D measurement device for quality control of aircraft rivet', *Int. J. Computational Vision and Robotics*, Vol. 14, No. 1, pp.1–17.

**Biographical notes:** Benjamin Bringier is an Associate Professor at the University of Poitiers (France) and the XLIM Institute (CNRS UMR 7252). His research focuses on computer vision and image understanding. His interests concern the acquisition and reproduction of colour images for colourimetric and shape inspection with applications in roughness measurement, colour management, and multi-spectral imaging. In 2002, he joined the French National Laboratory for Metrology and Testing (LNE) as a PhD student and he received his PhD in 2005 from the University of Poitiers.

Majdi Khoudeir is a Professor in the XLIM Research Institute UMR CNRS 7252 at the University of Poitiers, France, since 1993. He received his PhD in optoelectronics from the University of Poitiers in 1990. His primary

area of research includes computer vision and image processing for surface inspection. He has published more than 70 publications in international journals and in proceedings of international conferences of repute.

## 1 Introduction

The aviation industry uses rivets extensively to secure the various parts of an aircraft. Thus, up to several thousand rivets are attached to the exterior surface of the aircraft: the aircraft skin in the remainder of this article. Incorrect installation of these rivets is problematic for the aerodynamics of the aircraft and causes paint peeling when the aircraft is in flight, known as 'rivet rash' (Boeing Environmental Technotes, 2003). Verifying the positioning of each rivet on the aircraft skin is, therefore, a major issue and at this time no acquisition device allows quality control of all of them under acceptable conditions. Indeed, the ideal device must detect defects of the order of 100 $\mu$m, must be as fast as the installation of a rivet (about two seconds). This device must be light to be mounted on a robotic arm and handy enough to measure the different parts of the aircraft. Finally, it should be at the lowest possible price. As shown in the cross-section of a rivet in Figure 1, a single measurement point or along a line in 3D is not sufficient to determine the incorrect positioning of a rivet relative to the aircraft skin. Indeed, if the rivet is entirely too deep or the reverse (left and right cases in Figure 1), it is not necessary to worry about the position of the measures. Conversely in the middle example, the entire rivet surface must be measured to determine its positioning.

**Figure 1** Example of poorly positioned rivets relative to the aircraft skin (see online version for colours)

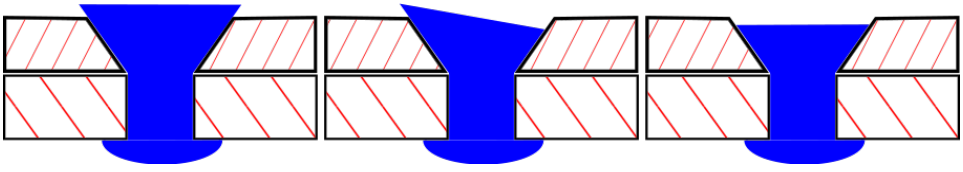

Many approaches are proposed in the literature to measure manufactured parts. The coordinate measuring machines where touch probes work by making contacts with the measured part are commonly used in industry for monitoring manufacturing processes and inspection of product specifications. These devices are generally very accurate (Ferreira et al., 2013) but require a very long acquisition time, which is not compatible with quality control with high throughput. Thus, optical devices which are contactless are generally preferred. Optical three-dimensional surface metrology techniques used in the industry could be classified into three categories: structured light, triangulation, and time of flight. The structured light technique has been invented in the 1980s (Creath, 1988). Periodic sinusoidal fringe patterns are projected onto an inspected surface and 3D reconstruction is obtained from fringe pattern modulation analysis. This method has been widely used and improved to increase its accuracy (Shoji et al., 2019; Wang, 2014) or its ease of use (Li and Wang, 2021). Specific fringe patterns besides sinusoidal phase patterns have been used (Van der Jeught and Dirckx, 2016) but the one-shot

structured light technique (Chen and Gool, 2019; Huang and Tang, 2014) does not allow to have a sufficiently accurate reconstruction for our problem. A multi-frequency phase-shifting scheme remains too slow and is generally problematic for shiny surfaces (Hu et al., 2019; Xu et al., 2020). The structured light technique could broadly include interferometry device (Hecht et al., 2002) which is often the choice for microscale 3D surface metrology. Interferometry devices are sensitive to environmental disturbances and are not realistically feasible for measurements directly on aircraft skin. When accuracy is not the primary concern, time of flight surface measurement techniques can be appealing (Hansard et al., 2012). The principle of time of flight depth sensing is to send an infrared wave directly to the target surface and the sensor detects the reflected light. The distance is calculated by measuring the phase difference between emitted and received infrared waves. Triangulation-based surface measurement is landed between structured light and time of flight techniques. Like the structured light approach, the active triangulation technique is invented in the 1980s (Bertani et al., 1984) where a photodetector array is used to locate a luminous point. Triangulation is generally not regarded as a state of the art method but as a minor approach specially used for measuring distances. In recent years, laser triangulation devices have been increasingly used for quality control in the field of automobiles (Tuononen, 2011), automation (Brosed et al., 2011) or construction (Giri and Kharkovsky, 2016) due to their high efficiency and low-cost. Unfortunately, the measurement environment and the surface appearance can interfere with the data acquisition accuracy. Many articles provide a state of the art of all of these techniques and make it possible to take stock of their qualities and issues (Marrugo et al., 2020; Wang, 2020; Bogue, 2010). Despite a large number of non-contact measurement methods, there are none to control the positioning of a rivet on an assembly line. Fairly accurate methods are generally reserved for laboratory use. Quick methods are generally not accurate enough (Bonin et al., 2021) to measure the positioning of a rivet and limit the problems of 'rivet rash'.

### *1.1 Our contributions*

In this paper, we propose a new methodology to acquire and analyse the positioning of a rivet about the aircraft skin. The proposed approach is close to triangulation methods and uses only one camera and two grid pattern projectors. Because all misplaced rivets must be detected, two projectors must be used to avoid failed detection, as explained in Subsection 2.2. The objective is to meet all the constraints: speed of acquisition and processing, manageability of the device, accuracy even if the environmental conditions change, and being inexpensive compared to existing devices. More specifically, the contributions of this paper consist of:

- The proposed device allows up to 2,000 measuring points on the aircraft skin and up to 600 measuring points on a rivet head of 1 $cm^2$ size with 10 $\mu$m of accuracy.
- Only one acquisition is necessary and the algorithms are very simple and fast, which makes it possible to check a rivet in less than two seconds. In addition, the final result directly indicates the position of the rivet with respect to the aircraft skin. It is thus possible to indicate whether part or all of the rivet is out of tolerance.

- Its compact and lightweight design makes it equally ideal for the field of the aviation industry and allows it to be mounted on a robot arm. The optical design avoids adjustments for each acquisition, only one calibration of the device is necessary for a series of measurements.

Our results show the accuracy of the proposed device even if the appearance of the surface is changed. The remainder of the paper is organised as follows. Section 2 presents the optical setup of our device. Section 3 describes the device calibration, the algorithm to obtain measuring points, and the quality control step. Section 4 presents our results for a comparative study and various cases including material appearance variation and device re-positioning study. Conclusion and future work are provided in Section 5.

## 2 Optical setup

As shown in Figure 2, the optical setup is composed of two grid pattern projectors and one sensor. The acquired area represents a rectangle of size 20.187 by 14.785 mm. To avoid measurement errors due to perspective projection calibration and imprecise device positioning, bi-telecentric lenses are used for sensor and projectors.

**Figure 2** (a) Diagram of the measuring head and the associated surface element (1) which is measured, the hardware setup consist of two LED projectors (2) with grid pattern and bitelecentric lens (3), a RGB camera (5) with a bitelecentric lens (4) (b) The device mounts on a robot arm (see online version for colours)

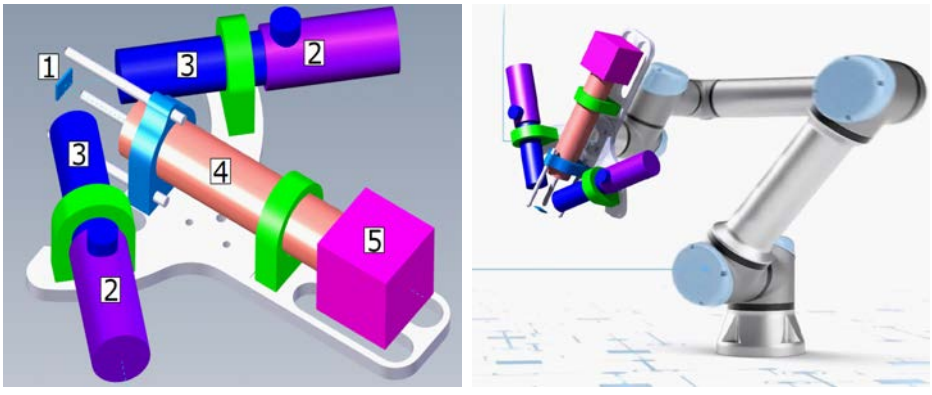


(a) (b)

This type of lens has negligible optical distortions and allows to obtain a very accurate metrology device (Niu et al., 2018). The weight of the device is about 3 kg, which is light enough to be mounted on a robotic arm. The size of this device is less than 20 by 30 cm, which corresponds to the same size as drilling or rivet positioning tools. Finally, the device must be positioned at a distance of 3 cm from the rivet to be analysed and the power consumption is less than 15 W.

### *2.1 Grid pattern projector*

Grid pattern projectors are composed of a 3 W power LED, a pattern positioning mechanism, and a bi-telecentric lens (Figure 2). According to Figure 5, the two grid pattern projectors and the sensor are in the same plane; If the $\varphi$ angle of the first projector is equal to 0, the $\varphi$ angle of the second one is equal to 180°. The $\theta$ angle is fixed to 45° for both projectors. To ensure that the projected pattern onto the surface is sharp over the entire analysed surface, the Scheimpflug principle must be respected (Figure 3). The grid pattern is therefore mounted on tilting support which makes it possible to obtain a single intersection point between the lens plane, the surface plane, and the projector plane.

**Figure 3** The Scheimpflug principle applied to line projector (see online version for colours)

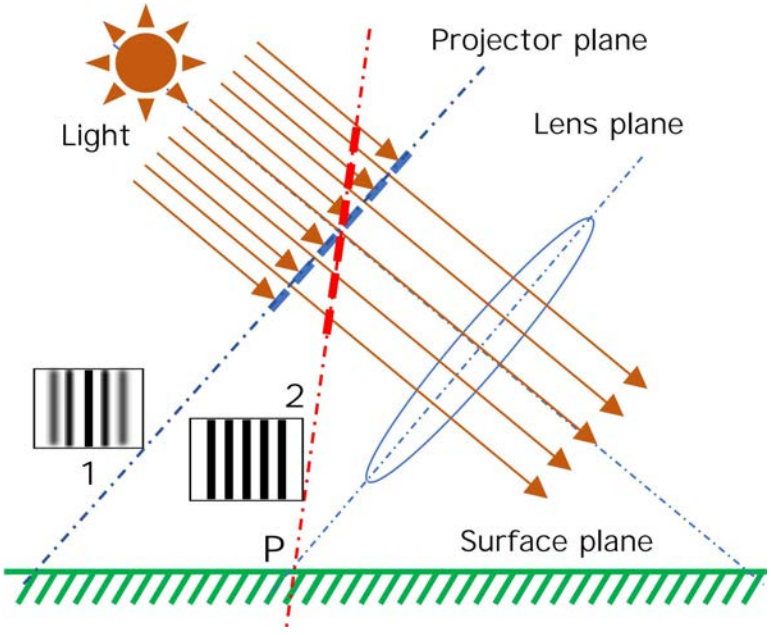


Notes: In case 1, the projector plane and the lens plane are parallel which produces blurred lines. In case 2, the projector plane, the lens plane and the surface plane meet at one point P which ensures that all lines are sharp.

The first projector emits in the red (a Gaussian centred to 630 nm) and has a grid pattern of 53 by 53 lines with a thickness of 50 $\mu$m and spaced 100 $\mu$m apart. The second one emits in blue (a Gaussian centred to 460 nm) and has a grid pattern of 32 by 32 lines with the same thickness but 200 $\mu$m apart. For both, the magnification of the bi-telecentric lens is equal to 0.528.

### *2.2 Sensor*

The sensor used for the following device is composed of a Sony IMX304 sensor with a pixel size of 3.45 $\mu$m and a bi-telecentric lens with a magnification of 0.7. One-colour

pixel (i.e., a pixel with a red, green, and blue component) is obtained from 2 by 2 raw sensor pixels, the resolution for axes X and Y is thus 9.857 $\mu$m. Because the angle $\theta$ between the normal of the macro surface and the projector is equal to 45°, and both the sensor and projector have an orthographic projection, a displacement of one pixel in the image also corresponds to a height variation of 9.857 $\mu$m.

**Figure 4** Problematic measurement if the line spacing h of the grid pattern is the same as the height between the rivet and the aircraft surface (see online version for colours)

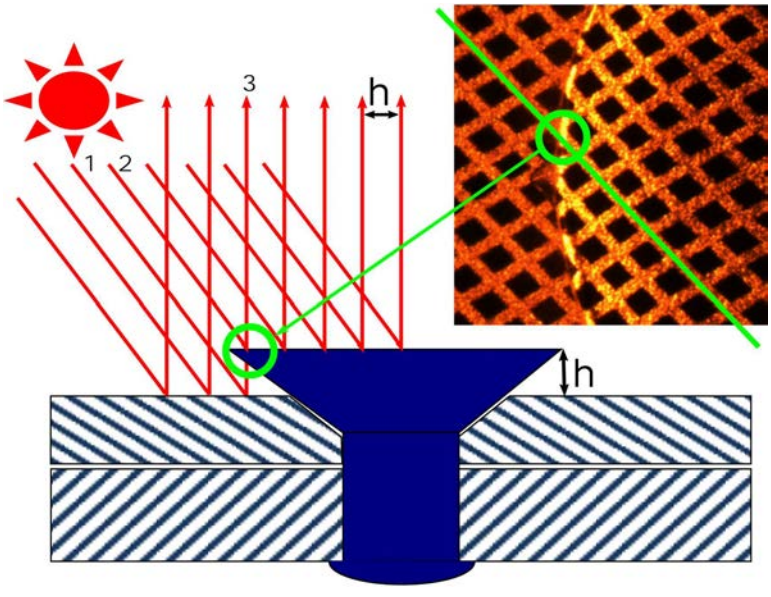


Notes: Two rays, 1 and 2 from the projector are confused by the sensor 3 as illustrated by a real acquisition from our system.

However, using a full orthographic projection system can be problematic if the height to be measured is equal to the spacing between the lines of the grid pattern. As shown in Figure 4, two different lines may be confused in the final image in this particular case. For this reason, the proposed device uses two grids with different line spacing to avoid failed detection. Because it is a colour sensor, separating the blue grid from the red one is very simple. The same algorithm is used on both gird and this approach allows parallel processing.

## 3 Controlling the rivet position

The control of rivet position must be accurate even if dust is on the sensor or the robot arm is not correctly positioned. In addition, a fast computing time is needed. The device is calibrated only once per series of measurements. A set of measurement points is extracted from every single photograph before being analysed to determine if the rivet is correctly positioned relative to the aircraft's skin.

### *3.1 Grid calibration*

To calibrate the device, it is necessary to determine three parameters (Figure 5):

1 the angle $\varphi$ which corresponds to the azimuth angle between the camera and the pattern projector

2 the angle $\theta$ which corresponds to the zenith angle between the camera and the pattern projector

3 the grid pattern positioning in the projector (angle $\beta$).

First and from the method proposed in Santo et al. (2020), we use the acquisition of a planar surface with small pillars whose geometric arrangement is known. From the cast shadow of each pillar on the planar surface, the angle $\varphi$ is calibrated. Then, we carry out the acquisition of a planar surface to calibrate the two other angles: $\theta$ and $\beta$. From the Fourier transform of the acquired image, the cross pattern $P$ (Figure 5) is created and the projected grid is estimated from the algorithm proposed in the following parts of this article. Because the angle $\varphi$ is already known, it is simple to estimate the angle $\beta$ which corresponds to the rotation of the pattern in the projector. Similarly, if the angles $\varphi$ ant $\beta$ are known, it is straightforward to calibrate the angle $\theta$ from the acquisition of the planar surface. Because the distance between each line of the grid is known and bi-telecentric lens are used, there is a sine relationship between the distance $h$ (Figure 4), the distance between two lines and the angle $\theta$.

**Figure 5** Representation of the angle $\theta$ and $\phi$ for the projector configuration and the grid pattern rotation $\beta$ inside the projector (see online version for colours)

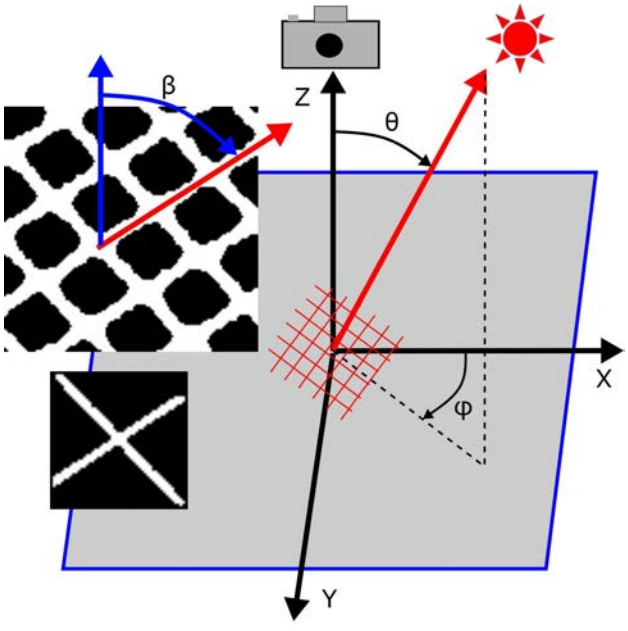


Notes: In inset (bottom left), the cross pattern $P$ used for measuring point detection.

The grid pattern $P$ obtained at this calibration step will be reused in the processing step of rivet acquisitions. As shown in the acquisition example in Figure 6, the surface around a rivet is generally flat and it is possible to redetermine a new pattern directly from a rivet acquisition if necessary.

### 3.2 Extraction of measuring point

The framework of processing the red or blue pattern is the same, the explanation of the proposed method will therefore be limited to the analysis of the acquisition of a rivet illuminated by the red grid. Figure 6 shows an example of one acquisition that will be used to explain the different steps of our algorithm. The problem exposed in Figure 4 does not occur in this example.

**Figure 6** Example of, (a) an image from our system for the red grid projector (b) an image with traditional light for a better understand (see online version for colours)

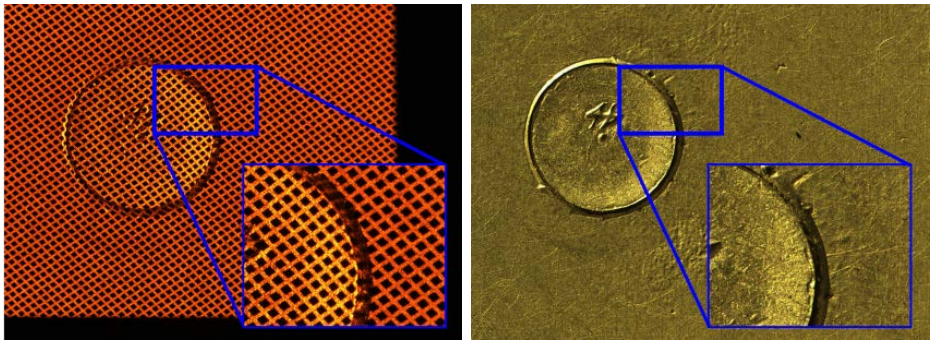

(a) (b)

The first processing step consists in extracting the position of each row and column crossing point of the projected grid. First of all, thresholding of red channel of the image is performed to obtain a binary image $I_b$. The histogram of the red channel is calculated and the threshold value is equal to 75% of the average of the higher 25 percentiles. It should be noted that this threshold must not be redetermined for each acquisition and depends essentially on the camera setting or the light source intensity in the pattern projector. Next, a binary convolution between the red grid binarisation and the pattern obtained at the calibration step is performed:

$$I_c(x,y) = \frac{1}{4ab} \sum_{dx=-a}^{a} \sum_{dy=-b}^{b} P(dx,dy) \text{ and } I_b(x+dx, y+dy) \tag{1}$$

This approach is much faster than directly applying a non-binary convolution to the gray-scale image of the red grid. In practice, it is only necessary to check whether the image $I_b$ is at one at the positions where $P$ is equal to one. $I_c(x,y)$ is equal to 1 when the pattern $P$ completely covers the image $I_b$ at position $(x,y)$ and equal to 0 if there is no matching between the pixels of $I_b$ and the values at 1 of $P$. Simple thresholding of the resulting image and the calculation of the barycentres of each area

makes it possible to obtain precisely the position of each line crossing. The threshold value is set at 0.9, which corresponds to a 90% overlap between the pattern and the grid binarisation. Point detection is performed by an association of connected pixels into single entities (Hernandez-Belmonte et al., 2013). Then, the barycentre point of each entity is calculated. These final points correspond to the measurement points made on the rivet and the skin of the aircraft. The undetected measuring points correspond to shadow areas or sudden variations in height, usually on the edges or the impact point of the rivet.

**Figure 7** Example of the measuring point detection, (a) a zoom to the acquired image (b) grid segmentation (c) binary convolution with the cross pattern (Figure 5) (d) measuring point and a circle with radius representing the tolerance of 50 $\mu$m (see online version for colours)

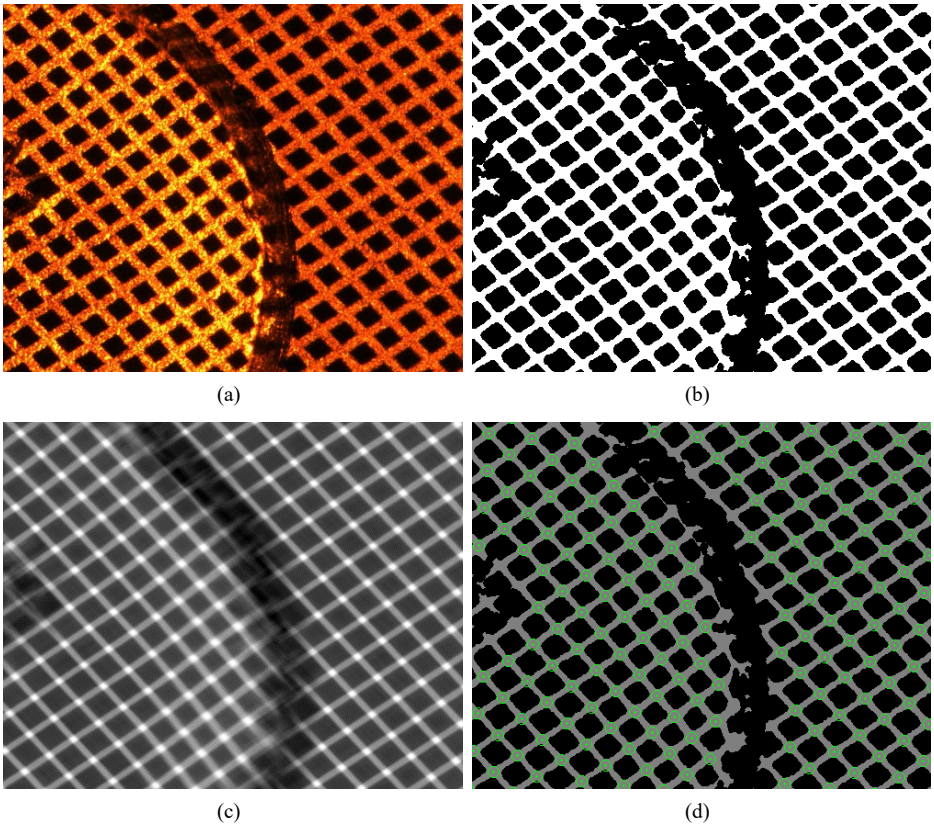


The next step of the framework consists of reconstructing the lines of the grid by differentiating, if possible, the area of the rivet and the aircraft skin. Starting from the bottom left corner of the image and for each measurement point obtained in the previous step, the proposed algorithm seeks to connect the current point $A_1$ to another named $A_2$ (Figure 8). Each measuring point is represented by a circle to allow a quick search, the centre of the circle corresponds to the measuring point and the radius to the search tolerance. Thus, a 2D ray-tracing algorithm and an accelerator structure can be used (Arvo and Kirk, 1989). A regular grid is used whose size of the sides of each cell

corresponds to the theoretical distance between three consecutive measurement points. From a point $A_1$, the search direction for ray tracing is calculated using angle $\beta$. Finally, the connectivity between $A_1$ and $A_2$ is tested by browsing and testing the pixels of the image $I_b$ on the line segment $A_1$ and $A_2$ using the Bresenham algorithm (Bresenham, 1965). If more than 10% of the pixels on the path are equal to 0, the two points are considered not connected.

**Figure 8** Connection algorithm between measurement points (see online version for colours)

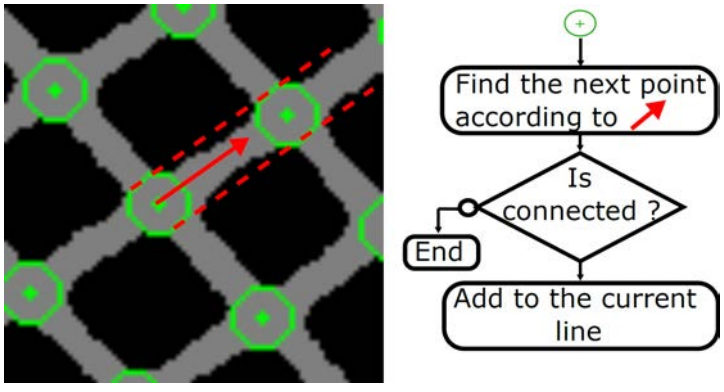


**Figure 9** Example of line reconstruction, (a) line segment obtained from the connecting algorithm (Figure 7) (b) the final grid reconstruction where green points are labelled out of the rivet and red points inside (see online version for colours)

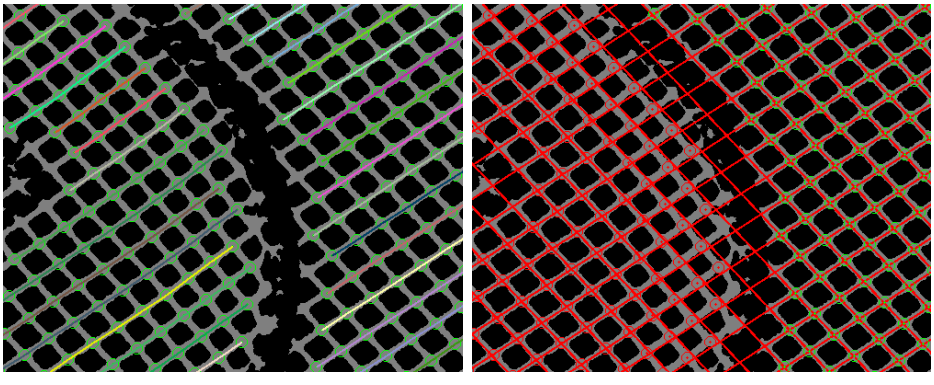

(a) (b)

If we consider that the rivet is always in the image centre which is a realistic assumption, the line segment closed to the pattern edges corresponds to the aircraft skin. Thus, by calculating their equation it is possible to link them together to reconstruct the grid pattern. The segments that are not connected correspond to the measurement points on the rivet. If all the segments are connected, it just indicates that the position of the rivet is in the same plane as the aircraft's skin. Then, it is possible to move to the next rivet. Figure 9 shows an example of line segment detection and grid pattern reconstruction. At the end of this step, we therefore obtain the reference plane which corresponds to the aircraft skin and the measurement points on the rivet.

### *3.3 Quality control*

The purpose of the quality control step is to check whether the rivet is not too deep in relation to the aircraft skin or vice versa. It is not possible to test a single point or a single line because the rivet may be positioned at an angle relative to the aircraft's skin. Thus each of the measurement points is verified independently of the others. For one measurement point, the theoretical position on the grid is searched in the direction of $\varphi$ or $-\varphi$. The closest point is always considered the correct one. Each measuring point is classified as in or out of tolerance. For a point out of tolerance, the neighbours are checked to see if it is potentially a false measurement. It is also possible to check if the measurements agree between the red and blue grids. Figure 10 shows the final result obtained for the example surface.

**Figure 10** (a) Illustration of measuring point control: green points are outside the rivet, red points are within the 100 $\mu$m tolerance, blue points are outside of the 100 $\mu$m tolorence and the yellow arrows show the distance between theoretical grid point and measured point (b) The final rivet quality control with the same colour meaning (see online version for colours)

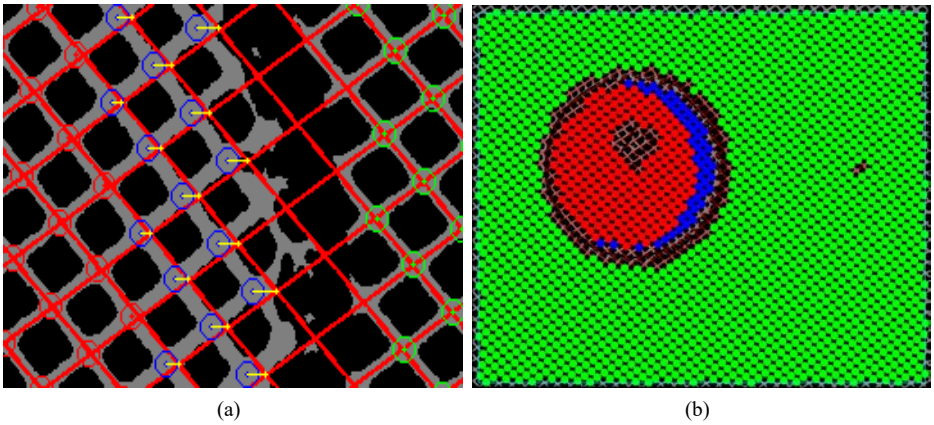

(a) (b)

The proposed algorithms are coded in C++ and without any optimisation (no multi-threading nor GPU computing), the acquisition and analysis time of a rivet is less than two seconds on a computer with an Intel Core I5-3550 processor at 3.3 GHz and 8 GB of memory. This time is less than the rivet setting time and allows a check of all rivets in parallel of aircraft manufacturing.

## 4 Experimental results

The proposed device is tested on two types of samples. First, a testing board with twenty rivets makes it possible to compare the results obtained between our device and a reference one. Secondly, our system is tested in real conditions on rivets placed directly on an aircraft door to test its robustness. Figure 11 shows a photograph of our device used in our experiments.

**Figure 11** A photograph of our prototype mounted on a robotic arm (see online version for colours)

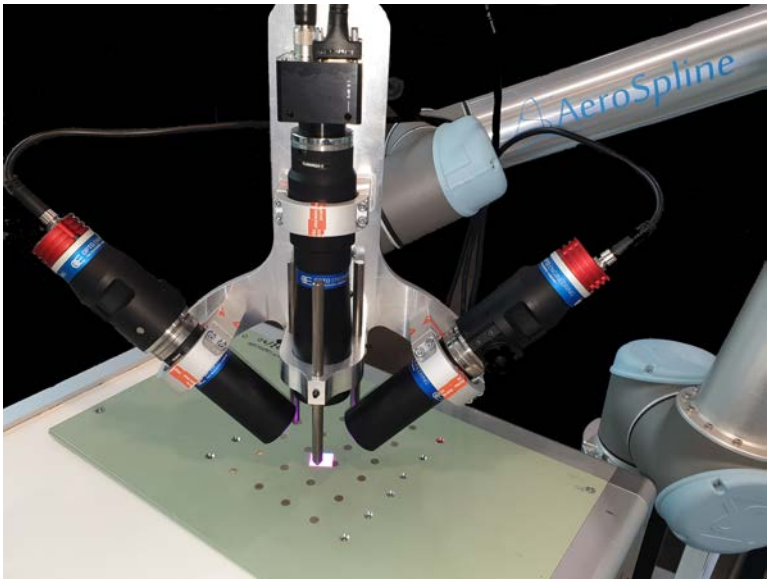


### *4.1 Comparative analysis*

To estimate the accuracy of the proposed method, a comparative study is carried out between the proposed device and the ZEISS CONTURA three-dimensional measuring device. Equipped with an RDS measuring head, the reference system has a measuring accuracy of 1.7 $\mu$m according to ISO 10360-5 standard (ISO10360-5, 2020).

**Figure 12** Rivet testing board to evaluate the accuracy of the proposed method (see online version for colours)

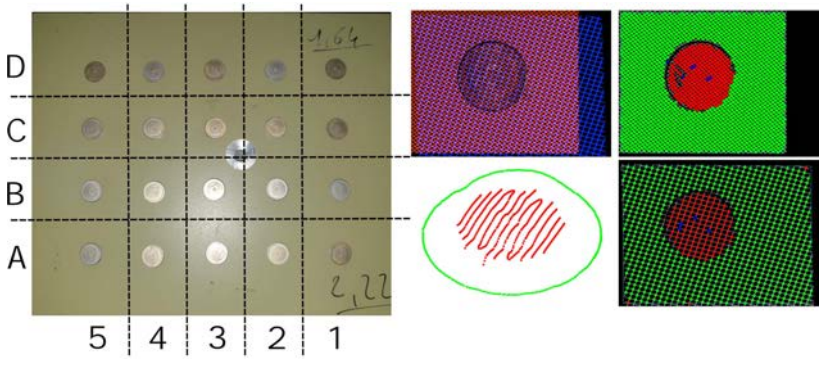


Notes: A photography of the board (top), an acquisition of rivet A-1 from our system (middle left), quality control from our method (middle and bottom right) and acquisition from ZEISS CONTURA device of rivet A-1 (bottom left).

Figure 12 shows the testing board used in this experiment which is made up of twenty numbered rivets from A to D along the rows and from 1 to 5 along with the columns. For each of them, a circular measurement made up of 298 points is made around the rivet to obtain a reference plane and a zigzag measurement is made up of 540 points on the rivet to check its positioning. An example of the measurement of the rivet A-1 by this methodology is shown in Figure 12. Our measuring device is also used to measure each rivet in order to compare the results between the two devices.

**Table 1** Comparison between our device and ZEISS CONTURA device, respectively first and second row of each cell: row and column index correspond to the rivet label in Figure 12

| | *5* | *4* | *3* | *2* | *1* |
|---|---|---|---|---|---|
| D | 23.5 (56.8) | 41.6 (67.9) | –15.2 (71.6) | 26.4 (49.4) | 64.1 (76.4) |
| | 34.2 (59.2) | 38.4 (88.7) | –24.2 (98.6) | 31.9 (59.2) | 71.2 (*108.4*; *0.4%*) |
| C | 51.6 (67.9) | 35.1 (76.8) | 71.6 (*159.4*; *3.1%*) | 37.4 (64.8) | 49.3 (68.4) |
| | 58.1 (78.8) | 29.4 (98.6) | 76.9 (*157.7*; *2.8%*) | 34.9 (88.7) | 56.1 (78.8) |
| B | –94.7 (*169.4*; *5.1%*) | 45.6 (79.8) | 69.1 (76.4) | –24.6 (81.6) | –67.3 (89.6) |
| | –96.6 (*177.4*; *5.2%*) | 39.1 (88.7) | 76.2 (88.7) | –33.2 (98.6) | –58.9 (88.7) |
| A | –52.6 (94.8) | –69.4 (*126.6*; *0.5%*) | 74.6 (*142.7*; *1.1%*) | 41.9 (69.5) | 88.6 (*152.3*; *2.1%*) |
| | –59.4 (88.7) | –67.9 (*108.4*; *0.4%*) | 71.1 (*137.9*; *0.9%*) | 45.2 (78.8) | 87.1 (*147.8*; *1.9%*) |

Notes: The first number corresponds to the average height of the rivet measuring point with respect to the reference plane. The number in parentheses is the absolute maximum distance. These distances are expressed in $\mu$m. The second number in parentheses corresponds to the percentage of points out of 100 $\mu$m tolerance.

Because it is impossible to do a point-to-point comparison between the two measuring devices, we first calculate the reference plane around the rivet (green measurement point in Figure 12) and then we calculate the average distance between this plane and all the measuring points on the rivet (red measurement point in Figure 12). For a better interpretation of the results, the absolute maximum distance is also calculated as well as the proportion of measurement points that exceed the tolerance of 100 $\mu$m. Table 1 presents the results for each rivet. For each cell, the first row corresponds to the measurement of the ZEISS CONTURA device and the second row corresponds to our device. These results show a strong correlation between the two measurement devices. The ZEISS CONTURA device has about six times the accuracy of our system, so it makes sense to have measurement deviations. The sign of the average distance error is always the same, thus it is possible to indicate if the rivet is broadly positioned under or above the aircraft's skin. More importantly, the maximum faults and the out-of-tolerance point detection rate are very similar. These results validate the proposed device to determine the positioning quality of a rivet with respect to an aircraft's skin.

### *4.2 Acquisition on real aircraft part*

When installing the rivets, the different parts of the aircraft can be covered with various paints that change the appearance of the surface. Figure 13 shows an example of appearance variation resulting from the surface with or without paint, these images come from a zoom of the acquisitions presented in Figure 14. At a scale close to a micrometer,

the light reflection when the material is raw is very erratic and there is plenty of glitter effect. When the surface is painted, the appearance is more diffuse and the grid pattern is more homogeneous.

**Figure 13** Example of appearance variation due to part with and without paint (see online version for colours)

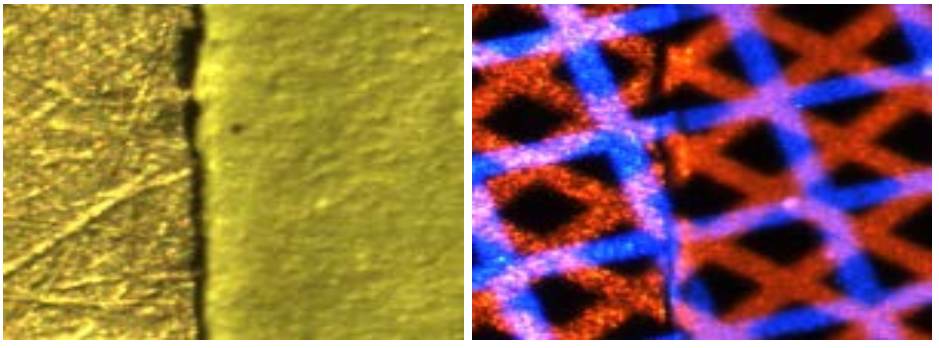

**Figure 14** Example of rivet quality control, (a) a photo of the rivet with traditionnal light (b) acquired image from our system (c) quality control with the red pattern (d) with the blue pattern (see online version for colours)

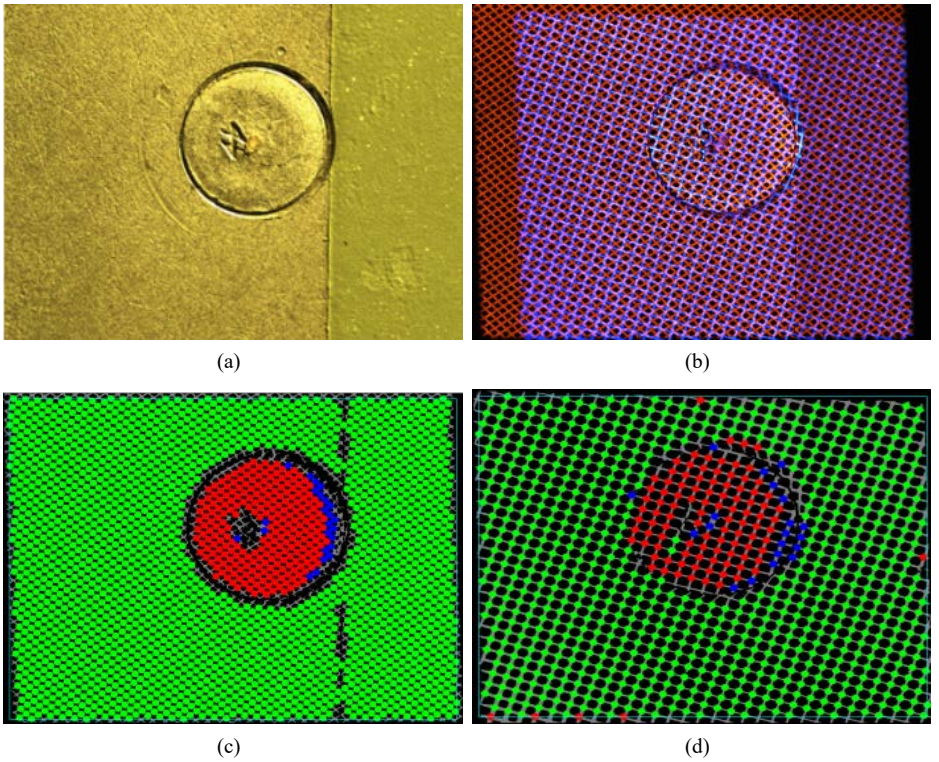

(a) (b)

(c) (d)

For a rivet positioned at the junction between a painted and unpainted area of an aircraft door, Figure 14 shows the result obtained at the output of our system. We can notice that the rivet is correctly controlled. Firstly, the grid pattern on the aircraft skin is correctly reconstructed. For the red projector, the difference in height between the parts with or without paint causes a shadow that does not disturb the analysis. Secondly, the results of the quality control from the red and the blue projector are consistent, the same out-of-tolerance areas are detected. The average height of the rivet from the aircraft skin is about 82 $\mu$m. The result demonstrates that the proposed system is not sensitive to changes in appearance, even when these changes occur in the same acquisition.

The second experiment consists in measuring the same rivet several times by re-positioning the system between each measurement. The example proposed in Figure 15 remains under the same unfavourable conditions where there is a changing appearance in the acquisition. In this example, the entire rivet surface is out-of-tolerance. For the two acquisitions in Figure 15, the average height of the rivet from the aircraft skin is the same and equal to 173 $\mu$m. For a set of three rivets and five measurements per rivet, the results obtained show a variation of the average error of less than 5 $\mu$m. This result shows that the measurements are perfectly reproducible and accurate.

**Figure 15** Example of rivet quality control: left and right rows are two measurements of the same rivet with acquisition device re-positioning (see online version for colours)

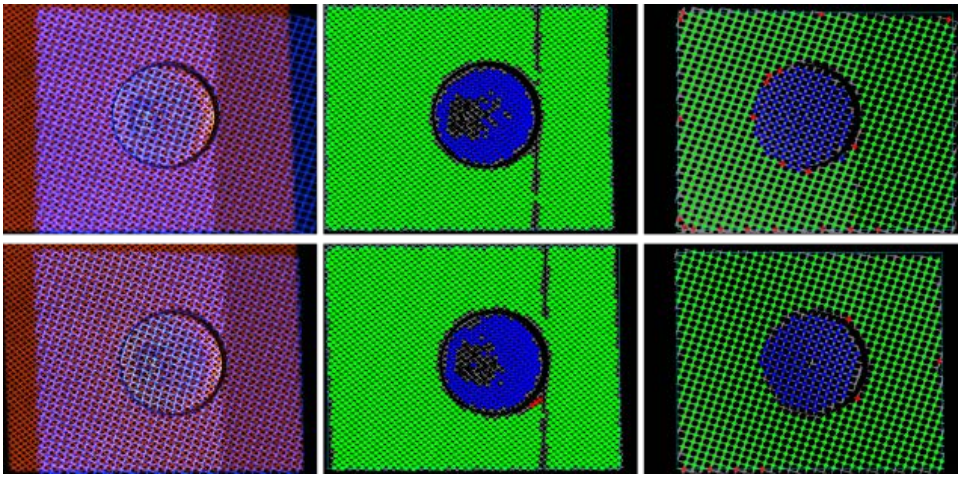

## 5 Conclusions

This paper presents a new fast and accurate device for quality control of aircraft rivet positioning. Incorrect rivet positioning is problematic for aerodynamics and causes paint peeling when the aircraft is in flight. Optical three-dimensional surface metrology techniques used in industry are typically too general to allow accurate measurement of all rivets on an aircraft. Our proposed methodology ensures a measurement time as fast as the mounting of one rivet and high measurement accuracy. Contrary to the traditional profilometer device which measures one line at a time, our device measures the entire surface of the rivet in relation to the aircraft skin from only one image acquisition. This device is lightweight and compact enough to be mounted on a robotic arm.

Our optical setup is very simple and uses traditional components, so it is very easy to duplicate it. Few parameters need to be calibrated and the measurement is insensitive to the positioning accuracy of the robotic arm. In the same way, various surface appearances do not disturbed the accuracy of our measure. As our results show, our device makes it possible to measure positioning errors of less than 100 $\mu$m for a measuring time of fewer than two seconds under real conditions of use. Currently, we are forced to use two projectors to avoid measurement errors when the line spacing of the grid pattern is the same as the height between the rivet and the aircraft surface. It would be interesting to use a coloured grid pattern to use only one projector. In Shuang and Wang (2021), an example of a coloured pattern projector is proposed but it is not accurate enough for our application. This approach would also simplify line detection for faster analysis.

## References

Arvo, J. and Kirk, D. (1989) *A Survey of Ray Tracing Acceleration Techniques*, pp.201–262, Academic Press Ltd., GBR.

Bertani, D., Cetica, M., Ciliberto, S. and Francini, F. (1984) 'High-resolution light spot localization with photodiode arrays', *Review of Scientific Instruments*, Vol. 55, No. 8, pp.1270–1272.

Boeing Environmental Technotes (2003) *Rivet Rash – The Itch that Won't Heal*, Vol. 8, No. 3, pp.1–4.

Bogue, R. (2010) 'Three-dimensional measurements: a review of technologies and applications', *Sensor Review*, March, Vol. 30, pp.102–106.

Bonin, R., Khameneifar, F. and Mayer, R. (2021) 'Evaluation of the metrological performance of a handheld 3D laser scanner using a pseudo-3D ball-lattice artifact', *Sensors*, March, Vol. 21, p.2137.

Bresenham, J.E. (1965) 'Algorithm for computer control of a digital plotter', *IBM Systems Journal*, Vol. 4, No. 1, pp.25–30.

Brosed, F., Aguilar, J., Guillomía, D. and Santolaria, J. (2011) '3D geometrical inspection of complex geometry parts using a novel laser triangulation sensor and a robot', *Sensors*, January, Vol. 11, pp.90–110, Basel, Switzerland.

Chen, X-L. and Gool, L.V. (2019) 'Watermarking structured light patterns for one-shot, extendable 3D scanning', in Wang, H. (Ed.): *Eleventh International Conference on Information Optics and Photonics (CIOP 2019)*, International Society for Optics and Photonics, SPIE, Vol. 11209, pp.1241–1254.

Creath, K. (1988) 'V phase-measurement interferometry techniques', in *Progress in Optics*, Vol. 26, pp.349–393, Elsevier.

Ferreira, F.A., de Vicente y Oliva, J. and Perez, A.M.S. (2013) 'Evaluation of the performance of coordinate measuring machines in the industry, using calibrated artefacts', *Procedia Engineering, The Manufacturing Engineering Society International Conference, MESIC*, Vol. 63, pp.659–668.

Giri, P. and Kharkovsky, S. (2016) 'Detection of surface crack in concrete using measurement technique with laser displacement sensor', *IEEE Transactions on Instrumentation and Measurement*, August, Vol. 65, pp.1951–1953.

Hansard, M., Lee, S., Choi, O. and Horaud, R. (2012) *Time of Flight Cameras: Principles, Methods, and Applications*, October.

Hecht, E. et al. (2002) *Optics*, Vol. 5, Addison Wesley, San Francisco.

Hernandez-Belmonte, U.H., Ayala-Ramirez, V. and Sanchez-Yanez, R.E. (2013) 'Enhancing CCL algorithms by using a reduced connectivity mask', in Carrasco-Ochoa, J.A., Martínez-Trinidad, J.F., Rodríguez, J.S. and di Baja, G.S. (Eds.): *Pattern Recognition*, Springer, Berlin, Heidelberg, pp.195–203.

Hu, Y., Chen, Q., Liang, Y., Feng, S., Tao, T. and Zuo, C. (2019) 'Microscopic 3D measurement of shiny surfaces based on a multi-frequency phase-shifting scheme', *Optics and Lasers in Engineering*, November, Vol. 122, pp.1–7.

Huang, B. and Tang, Y. (2014) 'Fast 3D reconstruction using one-shot spatial structured light', in *2014 IEEE International Conference on Systems, Man, and Cybernetics (SMC)*, pp.531–536.

ISO10360-5 (2020) 'Geometrical product specifications (GPS) – acceptance and reverification tests for coordinate measuring systems (CMS) – part 5: coordinate measuring machines (CMMS) using single and multiple stylus contacting probing systems using discrete point and/or scanning measuring moder', *ISO Standards Collection*, pp.1–45.

Li, Y. and Wang, Z. (2021) 'RGB line pattern-based stereo vision matching for single-shot 3-D measurement', *IEEE Transactions on Instrumentation and Measurement*, Vol. 70, No. 1, pp.1–13.

Marrugo, A.G., Gao, F. and Zhang, S. (2020) 'State-of-the-art active optical techniques for three-dimensional surface metrology: a review', *J. Opt. Soc. Am. A*, September, Vol. 37, pp.B60–B77.

Niu, Z., Gao, N., Zhang, Z., Gao, F. and Jiand, X.N. (2018) '3D shape measurement of discontinuous specular objects based on advanced pmd with bi-telecentric lens', *Opt. Express*, January, pp.1615–1632.

Santo, H., Waechter, M., Lin, W-Y., Sugano, Y. and Matsushita, Y. (2020) 'Light structure from pin motion: geometric point light source calibration', *International Journal of Computer Vision*, Vol. 128, No. 7, pp.1889–1912.

Shoji, E., Komiya, A., Okajima, J., Kubo, M. and Tsukada, T. (2014) 'Three-step phase-shifting imaging ellipsometry to measure nanofilm thickness profiles', *Optics and Lasers in Engineering*, January, Vol. 112, pp.145–150.

Shuang, Y. and Wang, Z. (2021) 'Active stereo vision three-dimensional reconstruction by RGB dot pattern projection and ray intersection', *Measurement*, January, Vol. 167, p.108195.

Tuononen, A. (2011) 'Laser triangulation to measure the carcass deflections of a rolling tire', *Measurement Science and Technology*, November, Vol. 22, p.125304.

Van der Jeught, S. and Dirckx, J.J. (2016) 'Real-time structured light profilometry: a review', *Optics and Lasers in Engineering*, December, Vol. 87, pp.18–31.

Wang, Z. (2014) 'Robust measurement of the diffuse surface by phase shift profilometry', *Journal of Optics*, October, Vol. 16, p.105407.

Wang, Z. (2020) 'Review of real-time three-dimensional shape measurement techniques', *Measurement*, May, Vol. 156, p.107624.

Xu, F., Zhang, Y. and Zhang, L. (2020) 'An effective framework for 3D shape measurement of specular surface based on the dichromatic reflection model', *Optics Communications*, November, Vol. 475, p.126210.